Commun. Theor. Phys. **76** (2024) 045601 (9pp) https://doi.org/10.1088/1572-9494/ad34c3

Diffusion of nanochannel-confined knot along a tensioned polymer*

Guobing Cai[1,4], Yong Li[1,4], Yuyu Feng[1], Zhouhui Deng[2] and Yanhui Liu[1,3]

[1] College of Physics, Guizhou University, Guiyang 550025, China
[2] Kechuang Industrial Development Company Limited, Guian New Area, Guiyang 550025, China
[3] State Key Laboratory of Public Big Data, Guizhou University, Guiyang 550025, China

E-mail: yhliu1@gzu.edu.cn

Received 6 January 2024, revised 27 February 2024
Accepted for publication 18 March 2024
Published 11 April 2024

Abstract

The knots frequently occur in biopolymer and their diffusion plays an active role in the gene regulation. In this work, Langevin dynamics simulations were carried out to detect the diffusion behaviours of a knot along a tensioned polymer in different spatial constraints. The polymer accommodating a knot was tethered to two macrospheres to block the unravelling of the knot. As a result, the curves for the diffusion coefficients of the knot with different bending stiffness as a function of the tension in different spatial constraints were obtained. In the space without constraints or with weak constraints, the corresponding curves for the knot with relatively large bending stiffness exhibited two turnover behaviours. On the contrary, for the knot with relatively small bending stiffness, the diffusion coefficients were monotonically reduced with increasing tension. However, in a space with strong constraints, all the curves showed one turnover behaviour regardless of the bending stiffness. The turnover behaviours divided the curves into different regimes, and the dominant diffusion mechanisms in the regimes, namely, knot-region breathing, self-reptation, and internal friction, were clearly identified. The effective friction coefficients ξ of the knots with 3_1, 4_1, 5_1 and 5_2 types as a function of the knot size N at a fixed tension were well fitted by the relation $\xi \propto N$. The effective friction coefficients of the knots at relatively large tension $f > 3$ sharply increased with the knot complexity, which is not dependent on the spatial constraints. By contrast, the values of these coefficients at relatively small tension $f \leqslant 3$ were remarkably dependent on the spatial constraints. Our work not only provides valuable simulation results to assist the understanding of the diffusion of DNA knot, but also highlights the single-molecule design for the manipulation of DNA knots in future.

Keywords: knot, langevin dynamics simulations, diffusion coefficient, self-reptation, knot-region breathing, internal friction

(Some figures may appear in colour only in the online journal)

1. Introduction

Knots are frequently found to occur in biopolymers, such as DNA molecules and proteins, and directly affect the gene regulation mechanisms [1–4]. For instance, knots can be *in vivo* introduced into cellular DNA *in vivo* through processes such as DNA replication and regulated by enzymes such as type II topoisomerases which both knot and unknot DNA [3, 4]. Knots can be artificially introduced into linear DNA by using single-molecule techniques and are intentionally proposed as a braking mechanism to improve the temporal resolution of nanopore sequencing [5–7]. In addition, the production of DNA knots *in vitro* has turned out to be a highly efficient manner to package mutant DNA into virus capsids [8]. Due to its biological functions and biophysical significance, knotted DNA serves as a minimal system to study the diffusion mechanism of molecular knotting and knot theory as applied to polymer physics [6, 9].

* The National Natural Science Foundation of China under Grant Nos. 11864006, 11874309, 12164007, and 12204118.
[4] These authors are contributed equally to this work.

The emergence of nanochannel techniques is arising as a powerful tool to deeply understand the knot diffusion in polymer [10–17]. In a series of experiments, one knot have been successfully introduced into a DNA molecule confined in a nanochannel and then stretched by an elongation force provided by divergent electric fields [18–21]. The knot appeared in the fully extended DNA as a region with excess fluorescent brightness. Its motion as a function of the applied tension rate could be tuned from a mobile to a jammed state and the knot jamming is reversible. Under these conditions, knots can be driven towards the closest end of the DNA molecule and untied. After shutting off the electric fields, knot swelling over time was also observed [21, 22]. A recent single-molecule experiment based on optical tweezers successfully introduced knots into an individual DNA molecule and manipulated the knot with applied tension. From the reported results, it was indicated that these knots, highly localized under tension, remained surprisingly mobile and underwent thermal diffusion [9]. The diffusion constants of the knots with different complexities were correlated with theoretical calculations concerning the knot sizes by using a simple hydrodynamical model of 'self-reptation' of the knot along a polymer [9, 13, 14, 23]. Nonetheless, in another experiment based on nanochannel, it was reported that self-reptation was not the only mechanism responsible for the diffusion. More specifically, it was suggested that an additional mechanism, namely breathing of the knot region, which involved the local exchange of stored length with the vicinal chain, is expected to dominate in relatively large knots, significantly increasing the knot diffusivity with quadratic scaling of the diffusion time [6, 10].

Motivated by the above-mentioned experimental results [9, 13, 14, 19, 21], a series of simulations were performed in this work to systematically study the diffusion of a knot along a tensioned polymer. From the acquired simulated outcomes based on Langevin dynamics, it was demonstrated that the knot diffusion coefficient was non-monotonically dependent on the tension at sufficiently large bending stiffness of polymer [24, 25]. However, the diffusion behaviours at low tension were not identified for the knot size comparable with the contour length of the polymer. At the same time, the underlying mechanism responsible for the diffusion of knots was clarified to better understand the physical processes enclosed in the experiments outlined in the above reviews. In the following simulations, the polymer confined in a nanochannel was tethered to macrospheres to prevent the unravelling of the knot from the polymer. Moreover, Langevin dynamics simulations were employed to detect the relationship of the various diffusion behaviours of a knot along a polymer in different spatial constraints as a function of the applied tension, especially at low tensions.

2. Materials and methods

2.1. Coarse-grained polymer model

As shown in figure 1(A), the simulation setup, which was composed of two macrospheres and a semi-flexible chain

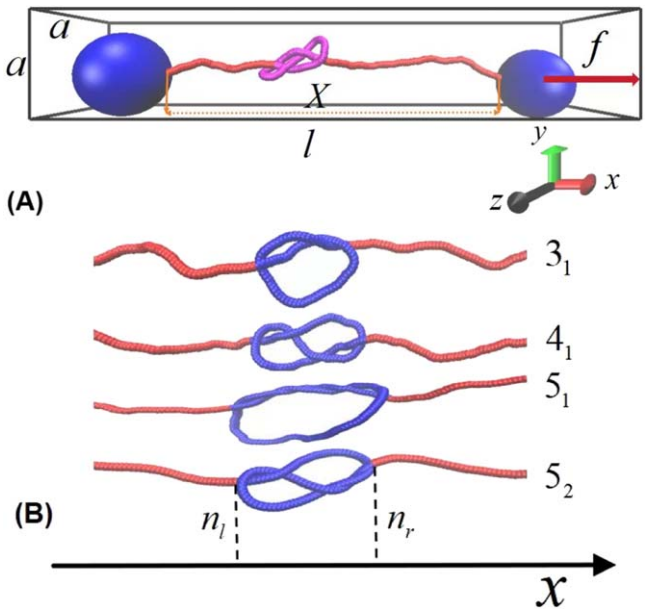

Figure 1. (A) Schematic illustration of the simulation setup: the ends of a polymer chain with 500 beads accommodating a 5_2 knot (highlighted in purple) are anchored to a macrosphere held fixed in the origin (left) and to a mobile one pulled along the x axis with a force $f = 0.5$. This simulation setup is confined in a cuboid nanochannel with length l, width a, and height a scaled by σ, and the length l is parallel to the x axis. (B) Typical conformations accommodating different knots (highlighted in dark blue). From up to down, the typical conformations represent a single knot 3_1, 4_1, 5_1, and 5_2, respectively.

accommodating knots with different types, was confined in a cuboid nanochannel. This semi-flexible polymer was modelled by a coarse-grained bead-spring model, which was composed of L monomers of diameter σ and mass m (σ and m are set as the unit of length and mass, respectively), and the contour length of the polymer used in current simulations is 500σ. Its two ends were tethered to two macrospheres, and the diameter of the two tethered macrospheres should be larger than the knot size to block the unraveling of the knot.

The interaction between two adjacent monomers in the semi-flexible polymer can be described by the finite-extensible nonlinear elastic (FENE) potential as follows

$$U_{\mathrm{FENE}} = -\sum_{i=2}^{L} \frac{1}{2} k_{\mathrm{FENE}} R_0^2 \ln\left\{1 - \left(\frac{r_{i,i-1}}{R_0}\right)^2\right\}, \quad (r_{i,i-1} \leqslant R_0) \tag{1}$$

It is a harmonic potential with a bond potential of $k_{\mathrm{FENE}} = \frac{30 k_{\mathrm{B}} T}{\sigma^2}$ and a maximum degree of stretching of $R_0 = 1.5\sigma$. These parameters were taken from the standard polymer model of Kremer and Grest [26], and $r_{i,i-1} = |\vec{r}_i - \vec{r}_{i-1}|$ is the distance between any pairs of monomers. At the same time, the bending potential between two adjacent monomers can be introduced as follows

$$U_{\mathrm{bend}} = \sum_{i=2}^{L-1} k(1 + \cos\theta_i), \tag{2}$$

where $\theta_i = -\arccos\left(\frac{\vec{b}_{i-1} \cdot \vec{b}_i}{|\vec{b}_{i-1}||\vec{b}_i|}\right)$ denotes the angle between

two adjacent bond vectors $\vec{b}_{i-1} = \vec{r}_i - \vec{r}_{i-1}$ and $\vec{b}_i = \vec{r}_{i+1} - \vec{r}_i$, and k refers to the bending stiffness. The equation $l_p = \kappa\sigma$ that correlates the persistence length l_p with the bond stiffness was applied to map the coarse-grained bead-spring model to dsDNA, and the parameters of hydrated dsDNA were adopted as $\sigma = 1.0$ nm and $\kappa = 50k_BT$.

In addition, the spatial interactions between any two monomers i and j were given by a short range truncated and shifted Lennard–Jones (LJ) potential U_{LJ} of strength ϵ with a cutoff distance $r_c = 2^{\frac{1}{6}}\sigma$ [27]

$$U_{LJ} = \sum_{i,j>i}^{L} 4\epsilon\left\{\left(\frac{\sigma}{r_{i,j}}\right)^{12} - \left(\frac{\sigma}{r_{i,j}}\right)^{6} + \frac{1}{4}\right\} \vartheta(2^{\frac{1}{6}}\sigma - r_{i,j}), \tag{3}$$

where $\varepsilon = k_BT$ is the unit of energy, and k_B and T denote the Boltzmann constant and the temperature, respectively.

To identify the impact of confinement on the diffusion of the knot along the semi-flexible polymer under tension, the interactions between monomers and the nanochannel were described as follows:

$$U_{wall} = \sum_{i=1}^{L} 4\epsilon\left\{\left(\frac{\sigma}{d_i}\right)^{12} - \left(\frac{\sigma}{d_i}\right)^{6}\right\}\vartheta(2^{\frac{1}{6}}\sigma - d_i), \tag{4}$$

where d_i is the orthogonal distance between the ith monomer and the nanochannel. Finally, the function $\vartheta(x)$ in equations (3) and (4) is the Heaviside function, can be defined as

$$\vartheta(x) = \begin{cases} 1 & (x<0) \\ 0 & (x \geqslant 0) \end{cases}. \tag{5}$$

2.2. Langevin dynamics simulations

During the dynamics, the macrosphere center and the chain ends were constrained to move along the x-axis [28]. A constant force f ($f = \frac{f_0\sigma}{\varepsilon} = \frac{f_0\sigma}{k_BT}$, in which $f_0 = \frac{\varepsilon}{\sigma}$) was also applied to the semi-flexible chain via two macrospheres, and the corresponding stretching potential was defined as $U_{stretch} = -\vec{f} \cdot \sum_{i=1}^{L}\vec{b}_i = -fX$. The x-axis coincides with the direction of the force f, and X is the projection of $\sum_{i=1}^{L}\vec{b}_i$ on the x-axis. The adimensional, reduced force f is typically varied in the range from 0.5 to 15 to characterize the mechanical tensile response of the knots under small, as well as large tensions. The model can explore a wide variety of polymer molecules with different values of l_p ranging from 1σ to 20σ, which correspond to polysaccharides and double-stranded DNA, and all of the simulations were performed at a constant temperature ($T = 1\frac{\varepsilon}{k_B}$). Since the macrospheres were free to rotate, and therefore no torsional stresses were generated in the simulations. The dynamics of the chain is generated by solving the Langevin equation as follows

$$m\ddot{\vec{r}}_i(t) = -\xi_0\dot{\vec{r}}_i(t) - \frac{\partial U_i}{\partial \vec{r}_i} + \vec{R}(t), \tag{6}$$

where U_i is the total potential of the ith monomer, including all the potentials mentioned above, and ξ_0 is the friction coefficient for each monomer and its value was set as $\xi_0 = 2\frac{m}{\tau_{LJ}} = 2\left(\frac{\sigma^2}{m\varepsilon}\right)^{-\frac{1}{2}}$, where $\tau_{LJ} = \sigma\sqrt{\frac{m}{k_BT}}$ is the Lennard–Jones time. The Stokes friction equation for a spherical monomer is given by the following expression: $\xi_0 = 3\pi\eta_{sol}\sigma$, in which η_{sol} is the viscosity of the solution. For a specified water viscosity $\eta_{sol} = 1cP$, $T = 300$ K, and $\sigma = 1.0$ nm, the characteristic Lennard–Jones time τ_{LJ} are related to $\frac{6\pi\eta_{sol}\sigma^3}{\varepsilon} \approx 1.14$ ns. In addition, $\vec{R}(t)$ is a stochastic force term that satisfies the fluctuation-dissipation theorem. Finally, the dynamical evolution of the system is numerically integrated with the LAMMPS package with an integration time step of $0.005\tau_{ij} \sim 5.7$ ps, and the total simulation time is about $10^8\tau_{LJ}$.

2.3. Knot detection and analysis

From a mathematically rigorous point of view, knots are defined only for closed chains. For our analysis, it is crucial to extend the knot notion to open chains by introducing appropriate schemes for joining the ends of the open chain by an arc and turning it into a closed ring. After closure, the physical knotted state of an open chain can be established by using the Alexander determinants [29], and the knotted portion of a chain is finally determined as the shortest chain segment that maintains the topology of the whole chain. The shortest chain segment is measured and identified based on a bottom-up searching scheme, which consists of three steps: (i) compute the center of mass of the portion, (ii) construct two segments starting from the ends of the portion and going far away from the center of mass and (iii) connect the termini of these segments at 'infinity'. Knots are designated by C_k, where C refers to the minimal number of self-crossings displayed when the knot is projected into a plane, and k denotes a cardinal index that is used to distinguish between topologically different knots with the same C [30]. In the current study, the Python package was employed to generate different knots. As shown in figure 1(A), a typical complex knot 5_1 is accommodated in a polymer under tension $f = 0.5$, and the other simple knots 3_1, 4_1, 5_1, and 5_2 are successively obtained, as demonstrated by figure 1(B).

3. Results and discussions

3.1. Impact of spatial constraints on the knot diffusion along a polymer

The diffusion of a knot along a polymer can be monitored by a discrete monomer index n, known as the diffusion coordinate. As indicated by the conformation with a 3_1 knot in figure 1(B), the boundaries of the knot region are defined as n_l and n_r, and the knot position along the chain is then defined as $n = (n_l + n_r)/2$. The knot diffusion coefficient can be identified by the following relationship $D = \langle[n(\triangle t) - n(0)]^2\rangle/(2\triangle t)$, where the square of the knot displacement $[n(\triangle t) - n(0)]^2$ is averaged over a series of short-time simulations, with the knot

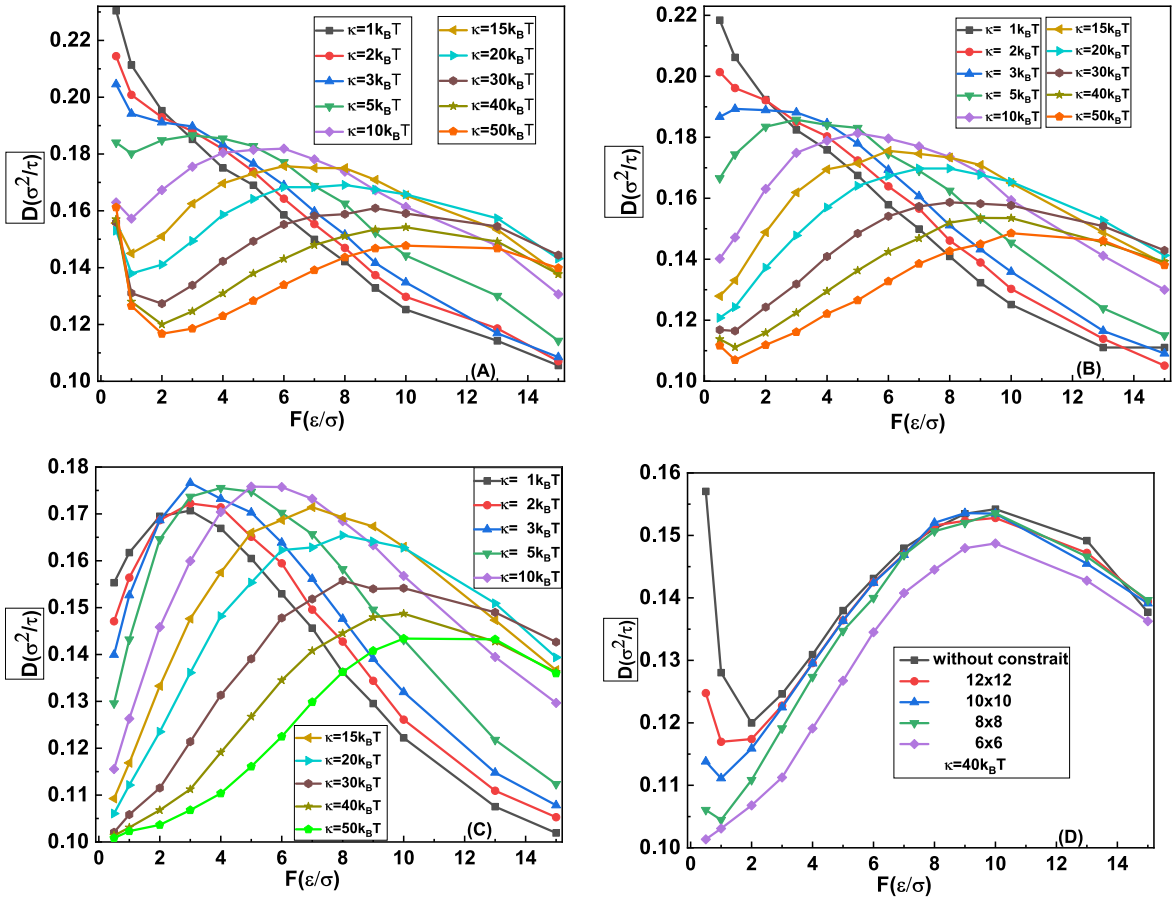

Figure 2. Impact of the spatial constraints on the diffusion coefficient of a 3_1 knot as a function of the tension f for different values of the bending stiffness κ. The spatial constraints corresponding to figures 2(A)–(C) are the space without spatial constraint, with $600 \times 10 \times 10$, and with $600 \times 6 \times 6$, respectively, and the contour length of the polymer is 500σ. (D) The diffusion coefficient of the 3_1 knot along a polymer with the bending stiffness $\kappa = 40k_BT$ as a function of the tension f changes with the spatial constraints.

initially located at $n(0)$ [25]. In the current simulations, the unraveling of the knot from the polymer is prohibited by tethering its ends to two macrospheres. Therefore, the diffusion coefficient in the low-force limit can be extracted from the current simulations [28]. According to this definition, the tension dependence of the diffusion coefficients of a knot with different bending stiffness k under different spatial constraints can be identified, and those of the 3_1 knot are demonstrated in figures 2(A)–(D), in which the knot diffusion coefficients and tension f are scaled by σ^2/τ and ε/σ, respectively. Furthermore, the dependence of the diffusion coefficients of a 3_1 knot along a polymer with the bending stiffness of $\kappa = 40k_BT$ on the spatial constraint is outlined in figure 2(D), in which the curves for the space without constraints or weak constraints have two turnover behaviours, and the first turnover behaviour becomes totally disappeared in the space with a strong constraint of $600 \times 6 \times 6$.

In the space without constraints and with weak constraints shown in figures 2(A) and (B), the diffusion coefficient of the 3_1 knot as a function of the tension f at relatively large bending stiffness $\kappa > 3k_BT$ exhibits a non-monotonic pattern. Their corresponding curves have two turnover behaviours and are divided into three regimes, namely, the regime before the first turnover behaviour, the regime between the two turnover behaviours and the regime after the second turnover behaviour. Their corresponding knot diffusion coefficient is first reduced, and then increased, and finally decreased as the applied tension f became bigger. Those at relatively small bending stiffness $\kappa \leqslant 3k_BT$ monotonically decreased with the increasing tension f.

In the regime before the first turnover behaviour, the diffusion coefficient of the 3_1 knot reduced with increasing tension, which can be reasonably argued based on the knot-region breathing. Particularly, this effect involves the exchange of the stored length locally with the vicinal chain and is expected to dominate in large knots. The increasing tension f gradually inhibits the knot-region breathing by reducing the knot size, consequently resulting in slower diffusion. This pattern is captured in figures 3(A)–(C), in which the relatively large knot in figure 3(A) is reduced to the relatively small one in figure 3(C) by increasing the tension from 0.5 to 2. When the knot conformation further developed into the loose knot corresponding to the regime between the two turnover behaviours (figures 3(D)–(F)), the 3_1 knot self-reptated along the polymer under tension and its diffusion coefficient D increased with the increasing tension. This effect could be interpreted considering that the knot diffusion is accomplished via a concerted motion of the loose knot.

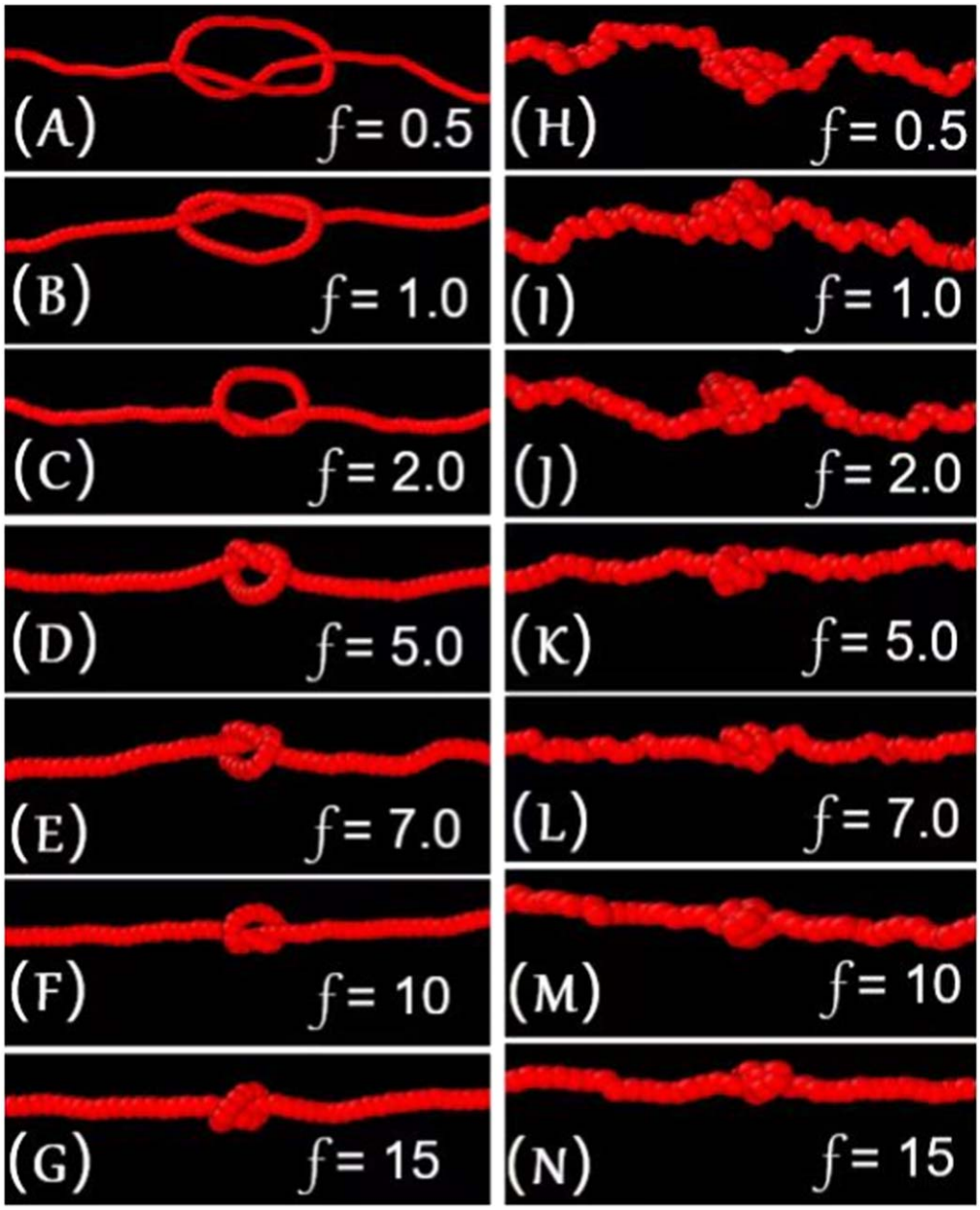

Figure 3. Typical conformations accommodate a 3_1 knot in a polymer under different tension in a space without constraints. (A)–(G) From up to down, the tension applied to the typical conformation with bending stiffness $\kappa = 50k_BT$ is 0.5, 1.0, 2.0, 5.0, 7.0, 10, and 15, respectively. (H)–(L) From up to down, the tension applied to the typical conformation with bending stiffness $\kappa = 1.0k_BT$ is 0.5, 1.0, 2.0, 5.0, 7.0, 10, and 15, respectively.

Hence, the total friction drag force that acts on the knot is proportional to the number N of monomers within the knot multiplied by the friction coefficient ξ_0 per single monomer. Thus the friction coefficient ξ can be approximated as $N\xi_0$, and the Einstein relation $D = k_BT/\xi$ for a knot can be re-expressed as $D \simeq k_BT/N\xi_0$, The increasing tension could also effectively accelerate the knot diffusion by reducing the knot size N.

When the loose knot was switched to the tight knot corresponding to the regime after the second turnover behaviour, the intrachain interactions within the tight knot enhanced the 'bumpiness' of the energy landscape of the knot, which is the microscopic origin of internal friction [31–34]. The application of a higher tension f induced a rougher energy landscape and consequently a slower diffusion. This assumption on the internal friction provided valuable insights for understanding the monotonic decrease of the diffusion coefficient of the 3_1 knot with relatively small bending stiffness $\kappa \leqslant 3k_BT$ as a function of the increasing tension f in the space without spatial constraints. As indicated by figures 3(H)–(J), because of the relatively small bending stiffness, the conformation of 3_1 knot under tension is directly developed into the tight knot. For this reason, the diffusion coefficient was gradually reduced by the internal friction.

In figure 2(C) with strong constraints of $600 \times 6 \times 6$, the curves are divided into two regimes by the second turnover

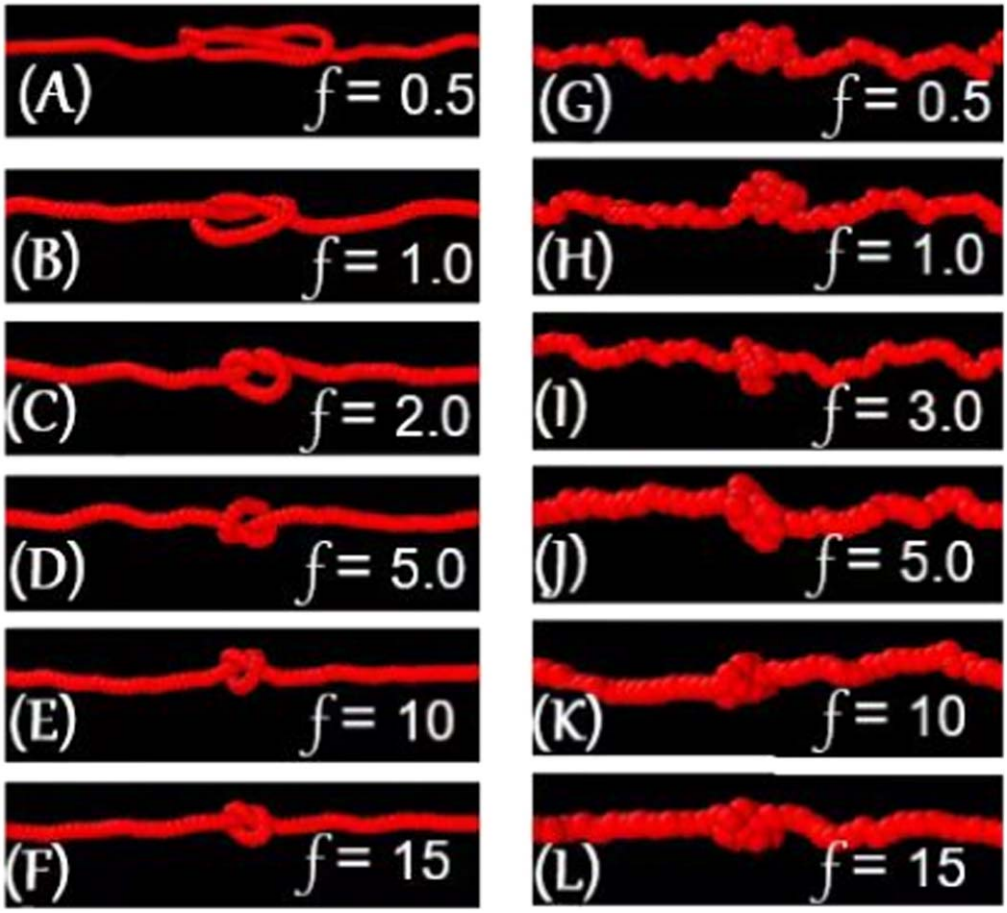

Figure 4. Typical conformations accommodating a 3_1 knot in a polymer under the application of different tensions in a space with the spatial constraint of $600 \times 6 \times 6$. (A)–(F) From up to down, the tension applied to the typical conformation with bending stiffness $\kappa = 50k_BT$ is 0.5, 1.0, 2.0, 5.0, 10, and 15, respectively. (G)–(L) From up to down, the tension applied to the typical conformation with bending stiffness $\kappa = 1.0k_BT$ is 0.5, 1.0, 2.0, 5.0, 10, and 15, respectively.

behaviour, namely, the regime before the second turnover behaviour, and the regime after the second turnover behaviour. In the regime before the second turnover behaviour, the change in the diffusion coefficient with the increasing tension could be ascribed to a similar assumption to that corresponding to the regime between the two turnover behaviours in the space without constraints or weak constraints (figures 2(A) and (B)). However, the conformation transition of the 3_1 under the strong constraints of $600 \times 6 \times 6$ is obviously different. As demonstrated by the typical conformations with large bending stiffness $\kappa = 50k_BT$ in figures 4(A)–(F), the 3_1 knot was compressed into the back-folding state (figure 4(A)) by the strong constraints. This effect resulted in the disappearance of the regime before the first turnover behaviour indicated in the space without constraints, namely, the knot-region breathing is inhibited by the strong constraints. The 3_1 knot in the back-folding state and its successive loose knot (figures 4(A)–(F)) self-reptate along the polymer, and their diffusion is accelerated by reducing the number of monomers within this knot. As a result, its corresponding diffusion coefficients are increased. In the regime after the second turnover behaviour, the diffusion coefficient decreased with the increasing tension, which can be also reasonably understood by the internal friction in a tight knot. As indicated by figures 4(E)–(F), by increasing tension f more than 10, the 3_1 knot switched from the transition state (figure 4(E)) to the tight knot (figure 4(F)). On top of that, the internal friction between the monomers within a knot, rather than the viscous friction due to the solvent, became gradually dominant over the knot diffusion, which induced the gradual reduction in the diffusion coefficients of the 3_1 knot in the transition state and its following tight knot. The implementation of a higher tension f reduced the diffusion of the knot, and even the 3_1 knot was almost jammed in the polymer, which was observed in current simulations and recent single-molecule experiments [9].

The conformation transitions of the 3_1 knot with relatively small bending rigidity $\kappa \leqslant 3k_BT$ in space with strong constraints of $600 \times 6 \times 6$ were different from those with relatively large bending rigidity $\kappa > 3k_BT$. As indicated by figures 4(G)–(L), the typical knot conformations with bending stiffness $\kappa = 1k_BT$ are directly developed into a loose knot by passing over the back-folding state, and then switched to the tight knot. Its corresponding diffusion coefficients first increased, and then decreased with the increasing tension f.

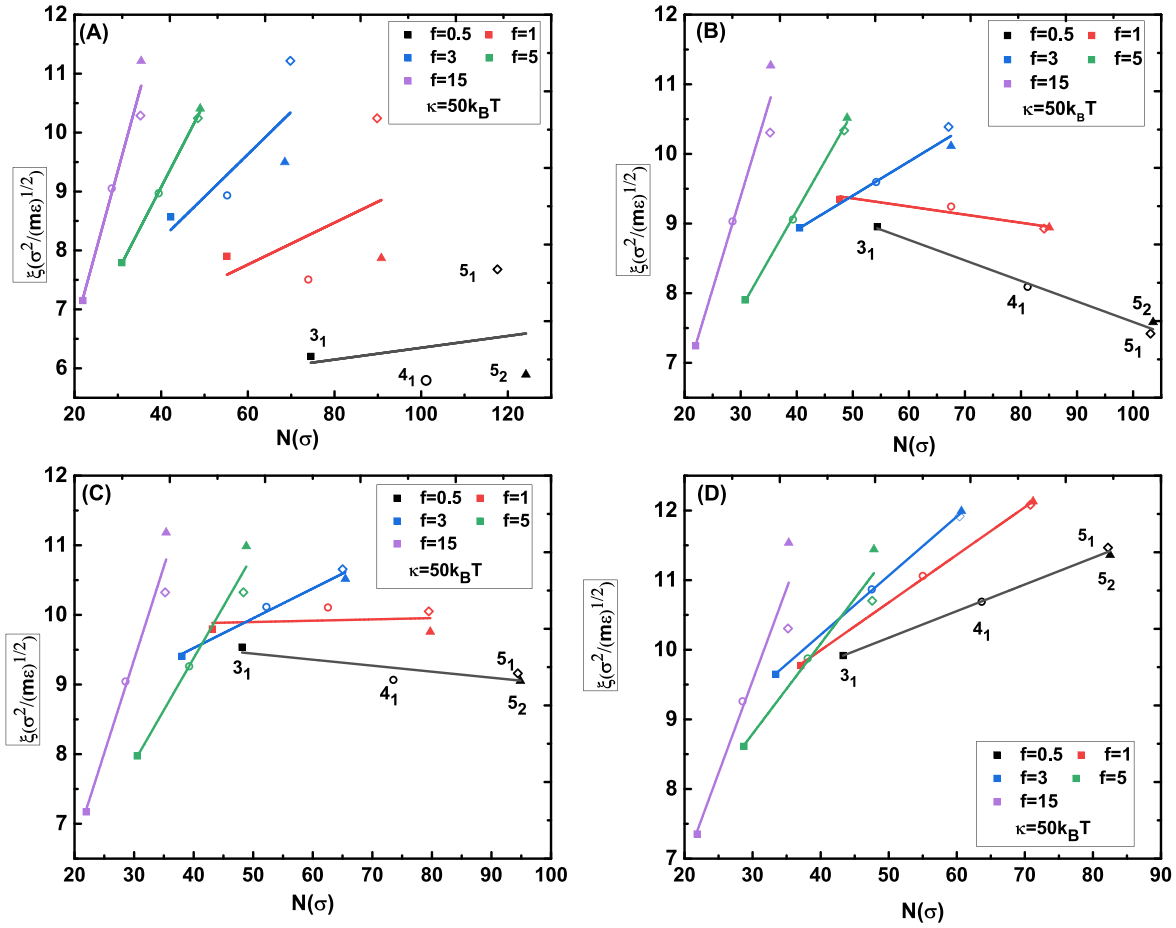

Figure 5. The effective friction coefficient ξ varies dramatically with the knot size at different tension in different spatial constraints. The spatial constraints corresponding to (A)–(D) are without constraints, with constraints of $600 \times 10 \times 10$, $600 \times 8 \times 8$ and $600 \times 6 \times 6$, respectively. The applied tension ranges from 0.5 to 15 and the bending stiffness of knot is $\kappa = 50k_BT$. The symbols of ■, ∘, ◊, and ▲ in different colors indicate the knots of type 3_1, 4_1, 5_1 and 5_2, respectively.

3.2. Effects of knot type on knot diffusion along a polymer

The diffusion coefficients for the knots with types of 3_1, 4_1, 5_1, and 5_2 and different values of κ, f under different spatial constraints were systematically computed. The results for the bending stiffness $\kappa = 50k_BT$ are outlined in figure 5, where the effective friction coefficients $\xi = k_BT/D$ of the knots of type 3_1, 4_1, 5_1 and 5_2 as a function of the knot size N at a fixed tension were well fitted by the relationship $\xi \propto N$, where the ratio ξ/N represents the friction coefficient ξ_0 of a single monomer [9, 25]. Moreover, some physical information enclosed in the knot diffusion can be drawn from the comparison among figures 5(A)–(D). More specifically, the effective friction coefficients of knots of type 3_1, 4_1, 5_1 and 5_2 as a function of the knot size N at relatively large tension $f > 3$ sharply increased with the knot complexity, which is not obviously dependent on the spatial constraints. By contrast, the effective friction coefficient ξ of knots with 3_1, 4_1, 5_1 and 5_2 types as a function of the knot size N at relatively small tension changing with the knot complexity is remarkably dependent on the spatial constraints. Take the relatively small tension $f = 0.5$ for example, in the space without constraints, the effective friction coefficients with 3_1, 4_1, 5_1 and 5_2 types as a function of the knot size N slightly increased with the knot complexity. With the gradual shrinking of the spatial constraints from $600 \times 10 \times 10$ to $600 \times 8 \times 8$, and then to $600 \times 6 \times 6$, their corresponding effective friction coefficients of knots with types of 3_1, 4_1, 5_1, and 5_2 as a function of the knot size N were obviously reduced, then slightly decreased, and finally sharply increased with the knot complexity. All these effects can be attributed to knot-region breathing and internal friction.

4. Conclusions

In this work, the Langevin dynamics simulations were employed to detect the diffusion behaviours of a knot along a tensioned polymer in different spatial constraints. Motivated by the optical tweezers experiment, the polymer accommodating a knot was tethered to two macrospheres, so that the unraveling of the knot from the polymer could be prohibited. According to this simulation design, not only the diffusion coefficient of the knot at different tensions was obtained including the low-tension limit, but also the diffusion mechanisms, namely, knot-region breathing, self-reptation, and internal friction.

The spatial constraints had an obvious impact on the diffusion of a knot as a function of tension f. In the space without constraints, the curve for the diffusion coefficients of a knot as a function of the applied tension f at relatively large bending stiffness $\kappa > 3k_BT$ was divided into three regimes by two turnover behaviours, and the knot-region breathing, self-reptation f. Because of the relatively small bending stiffness $\kappa \leqslant 3k_BT$, the knot was directly shrunk to a tight knot by the increasing tension f, and the internal friction began to dominate the diffusion of a tight knot and resulted in the monotonically reduced diffusion coefficients with increasing tension f. When the space was shrunk to the strong constraint of $600 \times 6 \times 6$ from the space without constraints, the curve for the diffusion coefficient of a knot as a function of tension f was divided into two regimes by the second turnover behaviour, where the self-reptation and internal friction were separately responsible for the increasing and decreasing of the diffusion coefficients of knot with the increasing tension f, and the knot-region breathing corresponding to the regime before the first turnover behaviour was inhibited by the strong spatial constraints, where the relatively large knot was compressed into the back-folding state, and then further shrunk with the increasing tension f, self-reptating along the polymer.

The effective friction coefficients ξ of the knots with 3_1, 4_1, 5_1 and 5_2 types as a function of the knot size N at a fixed tension could be well fitted by the relationship $\xi \propto N$. Moreover, the effective friction coefficients of the knots with 3_1, 4_1, 5_1 and 5_2 types as a function of the knot size N at relatively large tension $f > 3$ sharply increased with the increasing knot complexity, which is not obviously dependent on the spatial constraints. By contrast, the effective friction coefficient ξ of the knots with 3_1, 4_1, 5_1 and 5_2 types as a function of the knot size N at relatively small tensions changing with the knot complexity is remarkably dependent on the spatial constraints. All of which can be attributed to knot-region breathing and internal friction.

The above simulation results for polymer with bending rigidity $k = 50k_BT$ and $\sigma = 1.0$ nm could be mapped to dsDNA, and their corresponding results in strong spatial constraint with $600 \times 6 \times 6$ (figure 5(D)) demonstrated that the knot self-reptated along the dsDNA and its diffusion coefficient D increased with the applied tension f from 0.5 to 10.0 pN, at the same time, the effective friction coefficient ξ of knots with different complexity increased dramatically with their increasing knot size at a fixed tension. The strong spatial constraints used in current simulations are reasonably compared with the experiment conditions used in a recent single-molecule experiment in reference [9], in which the λ genomic DNA accommodating an individual knot was confined in a space with 6%(*w*/*v*)poly(ethylene glycol)(PEG, molecular weight 35 000) and manipulated by optical tweezers with the applied tension ranging from 0.1 to 2.0 pN. Under these conditions, although the knot became highly localized, it remained surprisingly mobile and underwent thermal diffusion with classical random walk statistics. The single-molecule experiment results indicated that the effective friction coefficient ξ of knot with different complexities correlated with theoretical calculations of knot sizes and this correlation can be addressed by a simple hydrodynamical model of 'self-raptation' of the knot along a dsDNA. Obviously, the simulation results are consistent with the single-molecule results in reference [9], these consistencies not only assists the understanding of the diffusion of knot along a dsDNA, but also highlights the single-molecule design for the manipulation of DNA knots in the future.

References

[1] Macgregor H C and Vlad M 1972 Interlocking and knotting of ring nucleoli in amphibian oocytes *Chromosoma* **39** 205–14

[2] Liu L F, Depew R E and Wang J C 1976 Knotted single-stranded DNA rings: a novel topological isomer of circular single-stranded DNA formed by treatment with Escherichia coli omega protein *J. Mol. Biol.* **106** 439–52

[3] Sogo J M, Stasiak A, Robles-MI M, Kramer D B, Hernandez P and Schvartzman J B 1999 Formation of knots in partially replicated DNA molecules *J. Mol. Biol.* **286** 637–43

[4] Hanke A, Ziraldo R and Levene S D 2021 DNA-topology simplification by topoisomerases *Molecules* **26** 3375

[5] Arai Y, Yasuda R, Akashi K, Harada Y, Miyata H, Kinosita K and Itoh H 1999 Tying a molecular knot with optical tweezers *Nature* **399** 446–8

[6] Metzler R, Reisner W, Riehn R, Austin R, Tegenfeldt J O and Sokolov I M 2006 Diffusion mechanisms of localised knots along a polymer *Europhys. Lett.* **76** 696–702

[7] Suma A and Micheletti C 2017 Pore translocation of knotted DNA rings *Proc. Natl. Acad. Sci. USA* **114** E2991–7

[8] Orlandini E and Whittington S G 2007 Statistical topology of closed curves: some applications in polymer physics *Rev. Mod. Phys.* **76** 611

[9] Bao X R, Lee H J and Quake S R 2003 Behavior of complex knots in single DNA molecules *Phys. Rev. Lett.* **91** 265506

[10] Mao R and Dorfman K D 2023 Diffusion of knots in nanochannel-confined DNA molecules *J. Chem. Phys.* **158** 194901

[11] Morrin G T, Kienle D F and Schwartz D K 2021 Diffusion of short semiflexible dna polymer chains in strong and moderate confinement *ACS Macro Lett.* **10** 1005–10

[12] Ma Z and Dorfman K D 2021 Interactions between two knots in nanochannel-confined dna molecules *J. Chem. Phys.* **155** 154901

[13] Ma Z and Dorfman K D 2020 Diffusion of knots along DNA confined in nanochannels *Macromolecules* **53** 6461–8

[14] Ma Z and Dorfman K D 2021 Diffusion of knotted DNA molecules in nanochannels in the extended de Gennes regime *Macromolecules* **54** 4211–8

[15] Micheletti C and Orlandini E 2014 Knotting and unknotting dynamics of DNA strands in nanochannels *ACS Macro Lett.* **3** 876–80

[16] Odijk T 2006 DNA confined in nanochannels: hairpin tightening by entropic depletion *J. Chem. Phys.* **125** 204904

[17] Dai L, Renner C B and Doyle P S 2016 The polymer physics of single DNA confined in nanochannels *Adv. Colloids Interface Sci.* **232** 80–100

[18] Di Stefano M, Tubiana L, Di Ventra M and Micheletti C 2014 Driving knots on DNA with AC/DC electric fields: topological friction and memory effects *Soft Matter* **10** 6491–8

[19] Klotz A R, Soh B W and Doyle P S 2020 An experimental investigation of attraction between knots in a stretched DNA molecule *Europhys. Lett.* **129** 68001

[20] Renner C B and Doyle P S 2014 Untying knotted DNA with elongational flows *ACS Macro Lett.* **3** 963–7

[21] Klotz A R, Soh B W and Doyle P S 2018 Motion of knots in DNA stretched by elongational fields *Phys. Rev. Lett.* **120** 188003
[22] Narsimhan V, Renner C B and Doyle P S 2016 Jamming of knots along a tensioned chain *ACS Macro Lett.* **5** 123–7
[23] Smith D E, Perkins T T and Chu S 1995 Self-diffusion of an entangled DNA molecule by reptation *Phys. Rev. Lett.* **75** 4146–9
[24] Vologodskii A 2006 Brownian dynamics simulation of knot diffusion along a stretched DNA molecule *Biophys. J.* **90** 1594–7
[25] Huang L and Makarov D E 2007 Langevin dynamics simulations of the diffusion of molecular knots in tensioned polymer chains *J. Phys. Chem.* A **41** 10338–44
[26] Kremer K and Grest G S 1990 Dynamics of entangled linear polymer melts: a molecular-dynamics simulation *J. Chem. Phys.* **92** 5057–86
[27] Weeks J D, Chandler D and Andersen H C 1971 Role of repulsive forces in determining the equilibrium structure of simple liquids *J. Chem. Phys.* **54** 5237–47
[28] Caraglio M, Micheletti C and Orlandini E 2015 Stretching response of knotted and unknotted polymer chains *Phys. Rev. Lett.* **115** 188301
[29] Podtelezhnikov A A, Cozzarelli N R and Vologodskii A V 1999 Equilibrium distributions of topological states in circular DNA: interplay of supercoiling and knotting *Proc. Natl. Acad. Sci. USA* **96** 12974–9
[30] Tubiana L, Orlandini E and Micheletti C 2011 Probing the entanglement and locating knots in ring polymers: a comparative study of different arc closure schemes *Prog. Theor. Phys.* **191** 192–204
[31] Kirmizialtin S and Makarov D E 2008 Simulations of the untying of molecular friction knots between individual polymer strands *J. Chem. Phys.* **128** 94901
[32] Caraglio M, Baldovin F, Marcone B, Orlandini E and Stella A L 2019 Topological disentanglement dynamics of torus knots on open linear polymers *ACS Macro Lett.* **8** 576–81
[33] Buvalaia E, Kruteva M, Hoffmann I, Radulescu A, Förster S and Biehl R 2023 Interchain hydrodynamic interaction and internal friction of polyelectrolytes *ACS Macro Lett.* **12** 1218–23
[34] Das D and Mukhopadhyay S 2022 Molecular origin of internal friction in intrinsically disordered proteins *Acc. Chem. Res.* **55** 3470–80